Simulation of hydraulic heave using the material point method

Farzad Fatemizadeh, M.Sc., University of Stuttgart, IGS
Univ.-Prof. Dr.-Ing. habil. Christian Moormann, University of Stuttgart, IGS
Prof. Dieter Stolle, Ph.D., McMaster University, Ontario

Seepage and the corresponding forces affect the stability of a soil and its constituents. Piping, erosion and the fluidization of non-cohesive soils, as well as sedimentation are phenomena that occur as a result of the seepage forces. Hydraulic heave is an example where most of these phenomena are present. Hydraulic heave can be studied via numerical simulations using the Finite Element Method (FEM) where the soil-water interaction can only be investigated until failure. Thereafter the solid grains and pore water start to undergo large deformations that FEM is often not capable of representing due to mesh tangling problems. In this work, the Material Point Method (MPM) is adopted to simulate the hydraulic heave phenomenon. MPM is a numerical tool, which naturally accommodates large displacements and the corresponding deformations of the continuum while avoiding the drawbacks of the classical Lagrangean FEM. An in-house program was developed for this study. The program was validated using a problem for which the analytical solution is known. Thereafter, the model was used to simulate a hydraulic heave experiment. The results from the experimental and numerical investigations are compared and concluding remarks are presented.

1 Introduction

For excavations below the groundwater level a dewatering strategy is normally adopted to lower the water level and keep the excavation dry. This results in a head difference (see Figure 1) that forces water under the wall into the excavation site. As the head difference increases, the seepage velocities and the corresponding seepage forces increase, which can destabilize the soil at excavation, as well as causing hydraulic heave.

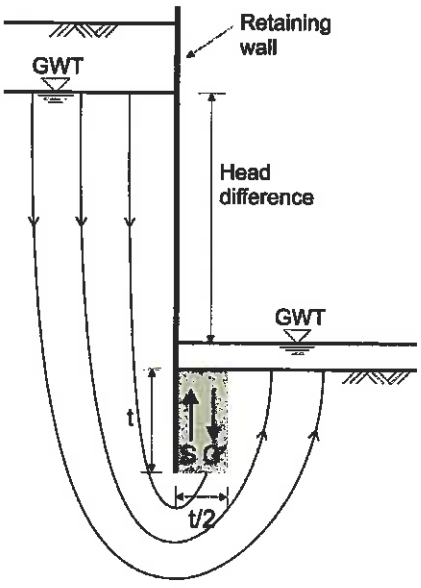

Figure 1: Hydraulic heave with Terzaghi's approach

This phenomenon is discussed in both the experimental and numerical literature. The experimental investigations go back to the work of Terzaghi at the beginning of twentieth century (Terzaghi 1925). There is considerable literature on this topic, including that of Koltuk (2017). His detailed experimental setup was capable of recording the pore water pressure in the sand along a retaining wall. He used Particle Image Velocimetry (PIV) to analyze the experimental data. Schober (2015) carried out detailed experimental investigations on hydraulic heave for excavations having a filter layer. He used the PIV method to identify the critical area near the retaining wall that is most likely to become unstable and provides detailed information about the failure process and the experimentally derived data. Alsaydalani and Clayton (2014) studied in their work the fluidization of sand beds subject to vertical seepage forces.

Hydraulic heave has also been examined using numerical models. Aulbach (2013) adopted two and three dimensional Finite Element (FE) models for a detailed investigation of the phenomenon and showed that the rectangular area adjacent to the retaining wall, which was assumed by Terzaghi as the region where hydraulic heave failure takes place, is a good simplification for the prism-like failure mass that develops in experimental and numerical tests. Benmebarak et al. (2005) employed the commercial software FLAC 2D for their simulations. They varied the soil parameters and considered their corresponding effects on the hydraulic head loss. Fonte (2010) made use of the software pack-

age Plaxis for their finite element simulations of hydraulic heave in excavations. He studied the behaviour of both fine and coarse grained soils, and compared the shape of failure for each soil type. Numerical methods other than Finite Element Method (FEM) have also been used; including, for example, Grabe and Stefanova (2015), who employed the smooth particle hydrodynamics method for their simulations, and Bolognin et al. (2017), who adopted the Material Point Method (MPM) for the simulation of fluidization in sand beds.

The classical Lagrangian FEM is capable of delivering results up to failure, but has difficulty to provide reliable information on the post failure behaviour of a liquefied soil. This is due to mesh tangling, which arises when dealing with large deformations. To avoid this problem, this study adopts the Material Point Method (MPM) to simulate hydraulic heave. MPM is a numerical tool which is naturally capable of accommodating large deformations of continuum, avoiding the shortcomings of Lagrangian FEM. The Material Point Method was developed for solid mechanics in 1990s by Sulsky et al. (1995) and Sulsky and Schreyer (1996). This method has been used to simulate different applications, including those in the field of geotechniques (Jassim 2013) and (Hamad 2014), to name a few. It has been adopted for the simulation of fully saturated soils; for example, by Jassim (2013) and Bandara (2013) who addressed problems dealing with saturated soils.

After a short review of the modelling framework and the governing equations for fully saturated soils in Section 2, a validation example, for which an analytical solution exists, is presented in Section 3. It is used to validate the in-house programme developed for this study. In Section 4, the hydraulic heave phenomenon is simulated and the results are discussed. Finally, Section 5 presents some concluding remarks.

2 Material point method

In MPM, a continuum is represented by material points (often referred to as particles), which act as "integration points" that move through a fixed background mesh. This feature enables MPM to represent the large deformations of the continuum and avoid the mesh tangling problem of classical Lagrangian FEM. The working procedure of MPM in one time step (Figure 2) consists of mapping the data stored on material points to the nodes of background mesh using standard shape functions (initialization phase). Thereafter the equations of motion are solved in the same manner as for classical FEM (solution phase). Finally, the data are mapped back to the particles using the same shape functions where the information is updated on the particles (convective phase).

Two strategies are available to represent a biphasic medium in the context of MPM. For the first approach a single particle set is used to define the solid and water phases where a part of the material point represents the solid phase and the other part the water phase based on the porosity (one point-two phase strategy). This method is adopted by e.g. Jassim (2013). For the second strategy each phase is represented by separate particle sets (two point-two phase strategy). This method was adopted previously by e.g. Bandara (2013). In this study the second method is employed (Figure 3) as it is better suited for the study of hydraulic heave. By adopting this strategy free water (free surface water), pore water and solid grains can be simulated in one model which is necessary for the investigation of hydraulic heave.

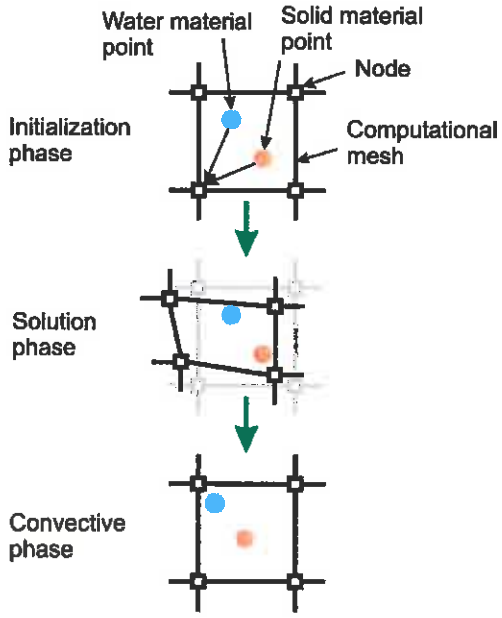

Figure 2: Working procedure of MPM

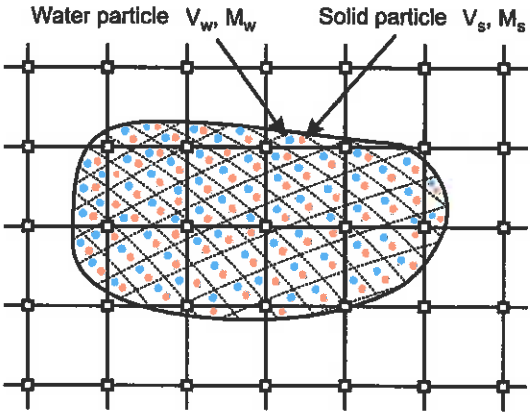

Figure 3: Discretization of MPM using two particle sets

The starting point for the two-phase dynamic MPM formulation considers the balance equations of momentum and mass. The momentum balance of the solid phase reads:

$$(1-n)\rho_s \boldsymbol{a}^s = \nabla \cdot [\boldsymbol{\sigma}' + (1-n)\boldsymbol{\sigma}_w] + \frac{n^2 g \rho_w}{k} \cdot (\boldsymbol{v}^w - \boldsymbol{v}^s) + \boldsymbol{\sigma}_w \cdot \nabla n + (1-n)\rho_s \boldsymbol{b} \quad (1)$$

where n is the porosity, ρ_s represents the solid grain density, $\boldsymbol{a}^s$ is the acceleration vector for the solid phase, $\boldsymbol{\sigma}'$ is the effective stress tensor and $\boldsymbol{\sigma}_w$ shows the water stress tensor for the free water, in which for the pore water it is replaced by pressure. The parameter g is the gravitational acceleration, ρ_w represents the water density and $\boldsymbol{k}$ is the permeability tensor. Homogenous isotropic soil is considered here, for which the permeability is independent of direction, thus $\boldsymbol{k}$ can be replaced by the scalar k. The variables $\boldsymbol{v}^w$ and $\boldsymbol{v}^s$ are the water and solid velocity vectors, respectively, and $\boldsymbol{b}$ is the body force per unit mass. The momentum balance for the water phase is written as:

$$n\rho_w \boldsymbol{a}^w = \nabla \cdot (n\boldsymbol{\sigma}_w) - \frac{n^2 g \rho_w}{k} \cdot (\boldsymbol{v}^w - \boldsymbol{v}^s) + \boldsymbol{\sigma}_w \cdot \nabla n + n\rho_w \boldsymbol{b} \quad (2)$$

where $\boldsymbol{a}^w$ is the acceleration vector for water. After deriving the weak form of the momentum balance equations and discretizing them in time and space, nodal accelerations for the solid and water phases are calculated separately. Thereafter, particle velocities are obtained by integrating the nodal accelerations explicitly and transferring them to material points. Particle velocities are mapped to the nodes to determine the nodal velocities by equating the momentum on the particles and nodes. In this stage, the mass balance equations of the solid and water are used to determine the water particle pressure keeping in mind that the solid grains are incompressible, with the water being slightly compressible and its density a function of pressure (fluid is assumed to be barotropic):

$$\frac{d}{dt}\mathrm{p} = \frac{K_w}{n}[(1-n)\nabla \cdot \boldsymbol{v}^s + n\nabla \cdot \boldsymbol{v}^w] \quad (3)$$

in which p is the water pressure and K_w represents the bulk modulus of water. The nodal velocities are now integrated implicitly in time to get the nodal displacements. Thereafter the strains are updated, depending on particle positions and on the nodal displacements; i.e.,

$$\delta\boldsymbol{\varepsilon}^\alpha = \mathbf{B}\delta\boldsymbol{u}^\alpha \quad (4)$$

where $\boldsymbol{\varepsilon}^\alpha$ is the strain tensor with $\alpha = s, w$ phases, $\mathbf{B}$ is the strain-displacement matrix and $\delta\boldsymbol{u}^\alpha$ is the nodal displacement vector of the α phase during the current time step. At this stage the constitutive law of the solid phase is called to update the effective stress tensor and the constitutive law of the water phase is called to update the stress tensor of the free water particles. The nodal displacements are also used to update the position of each particle for the next time step.

At this stage, it must be checked that the volume occupied by the water particles in each element does not exceed the value allowed by the porosity of that element. For the case in which this condition is violated, the pressure of the water particles in that element are increased depending on the mass balance of the solid phase:

$$\Delta\mathrm{p} = K_w\left(\frac{n_w}{n} - 1\right) \quad (5)$$

where Δp is the pressure correction due the violation of the water volume constraint and n_w is the actual porosity in the element. The parameter K_w is a large value. To eliminate drastic changes in pressure, a smaller value than K_w is adopted in equation (5) for this study.

3 Validation example

Based on the formulation discussed in Section 2, an in-house program code accommodating single particle and double particle sets was developed. In this study only the double particle set is adopted. To demonstrate the capability of the double particle set strategy to handle the two phases properly, the Mandel-Cryer effect is simulated. In this problem a homogenous, isotropic and linear elastic, fully saturated soil layer is confined between two rigid impermeable walls (Figure 4). A force is suddenly applied on the horizontal walls and the excess pore water pressure generation at the middle of the soil layer is tracked. For this problem an analytical solution exists in the literature (Cheng and Detournay 1988).

The soil layer is assumed to have a permeability of $k = 10^{-5}\,[m/s]$, porosity of $n = 0.4$, dry density of $\rho_d = 1680\,[kg/m^3]$, Poisson's ratio of $\nu = 0.3$ and constrained elastic modulus of $E_c = 5\,[GPa]$. Water is assumed to have a bulk modulus of $K_w = 2\,[GPa]$. The constrained elastic modulus of the soil is chosen to have the same stiffness in the soil and water so that the applied force is divided between water and soil equally at the beginning. The analytical solution is also derived for the case where solid matrix and water have the same stiffness.

Figure 5 shows the results obtained from the MPM simulation compared to that of the analytical solution for different dimensionless times. In this figure, the excess pore water pressure on the positive x-

axis (in the middle of the soil layer) is shown. Good agreement between the MPM simulation and the analytical results can be recognized.
The excess pore water pressure at the sides vanishes immediately whereas the excess pore water pressure in the middle of the sample, first increases (goes beyond 0.5) and then decreases with time. This is due to the fact that when the excess pore water pressure along the sides vanish, the system at both ends behaves softer than in the middle. Thus the external load is carried mostly by the particles at the middle of the system, which at first even shows an increase beyond the initial excess pore water pressure.

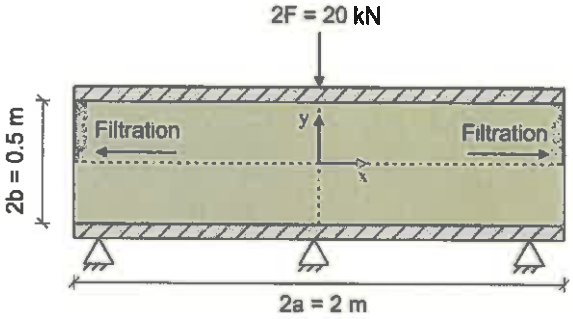

Figure 4: Geometry of the Mandel-Cryer problem

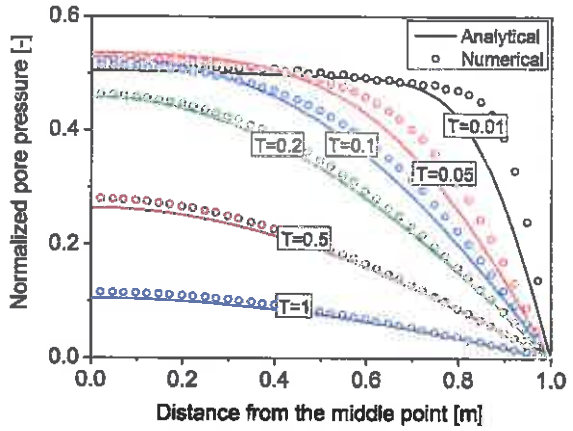

Figure 5: Results of the MPM simulation in comparison to analytical solution

4 Hydraulic heave

A series of tests were conducted at the Geotechnical Engineering Institute at the University of Stuttgart (Brandt 2015) to investigate the effect of construction errors for retaining structures on the initiation of hydraulic heave. An MPM model is constructed in this paper to simulate one of the laboratory tests, shown in Figure 6. Water was inserted into the sample at the bottom of the filter plate with a pipe that was attached to a water tank. The critical head difference in system at failure was recorded in experiment to be 23.05 cm. For the MPM model, the head difference for given the mesh size is assumed to be 24 cm.
The sand layer is modeled here as an elastic-perfectly plastic material following the Mohr-Coulomb failure criteria. Brandt (2015) provides some of the material parameters for the sand with the remaining values being assumed. The sand layer has a permeability of $k = 10^{-4}$ [m/s], friction angle $\varphi = 30°$, dilation angle $\psi = 5°$, cohesion $c = 0$ [Pa], grain density $\rho_s = 2650$ [kg/m³] and porosity $n = 0.4$. The Poisson's ratio is assumed to be $\nu = 0.3$ and elastic modulus has a value of $E = 10$ [MPa]. The filter plate is modeled as linear elastic material with permeability $k = 10^{-2}$ [m/s], porosity $n = 0.4$, density $\rho_s = 2650$ [kg/m³], Poisson's ratio $\nu = 0.3$ and elastic modulus $E = 10$ [MPa]. Water is assumed to have a bulk modulus $K_w = 20$ [MPa] and viscosity $\mu = 10^{-3}$ [Pa · s]. The bulk modulus of water is reduced by a factor of 1000 to increase the critical time step size needed for the dynamic simulations.
At first, the valve at position AB (Figure 6) was closed so that the system could reach hydrostatic equilibrium. Thereafter the valve was opened and the water was allowed to flow through the filter plate into the system. In the MPM model the water pipe and the water tank are simulated to supply the head difference in the system as well as the water particles, which are needed to penetrate into the sand sample.

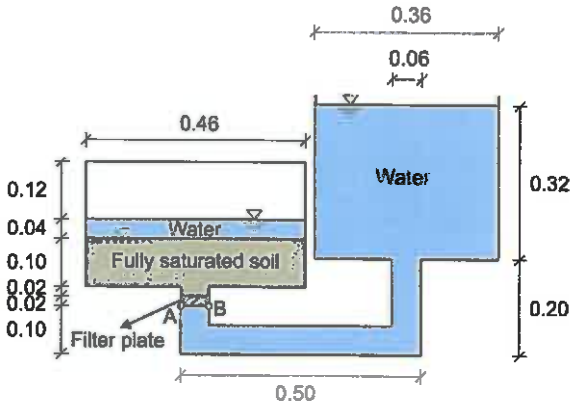

Figure 6: Geometry of the MPM model for hydraulic heave problem (all dimensions in meter)

Figure 7 shows the predicted displacement of the solid particles at different time stages after the opening of the valve. In this figure, the water particles are turned off to focus on the behaviour of sand, but it should be kept in mind that the sand is always fully saturated during the simulation (water stand is above the soil as it is the case in the experiments).

As can be seen in Figure 7, at the beginning the solid particles on the surface of the sand layer are fluidized due to the pressure waves applied from below on the sand and they start to swim in water. The particles on the surface are most affected by fluidization as there is no overburden pressure applied on them. The water particles coming from the water tank flows through the filter plate and push the sand layer upward. A small hole is produced above the filter plate (Figure 7 top). As time proceeds the produced hole becomes bigger and more solid particles from the sand surface become fluidized and swim in water. As discussed previously, the hole is filled with water and the water level increases as well above the sand. Finally the water particles push the sand layer completely upward and the phenomenon of hydraulic heave is completed. The prediction from the numerical simulation is in good agreement with the observations from the experiments shown in the literature, especially those of Brandt (2015) and Alsaydalani and Clayton (2014) where they observed the same failure procedure.

Figure 8 shows two pictures at two different time stages from the experiments of Brandt (2015) where the hole above the filter plate as well as failure state of the sand layer can be observed.

5 Conclusions

After a short discussion regarding hydraulic heave and reviewing some previous numerical and experimental studies, the material point method was described considering its advantages over the classical FEM. The two-phase formulation was presented in detail and the capability of an in-house developed computer program-code to capture two-phase, Mandel-Cryer effect was demonstrated by comparing predictions with the results from an analytical solution in literature.

Finally, an experiment completed at the University of Stuttgart to investigate hydraulic heave was simulated using the MPM program. The stages predicted by the simulation were also in good agreement with the observations of the laboratory experiment(s). The numerical model predicted almost the same head difference as reported for one of the experiments with regard to the critical value corresponding to the initiation of failure.

There are still some aspects that can be improved; e.g., the constitutive model adopted for soil and the corresponding material parameters should be investigated in more detail, and the potential mesh dependency of the predictions should be investigated. The comparison between the experiments and predictions must also carried out in more detail. All these points are currently being investigated by the authors.

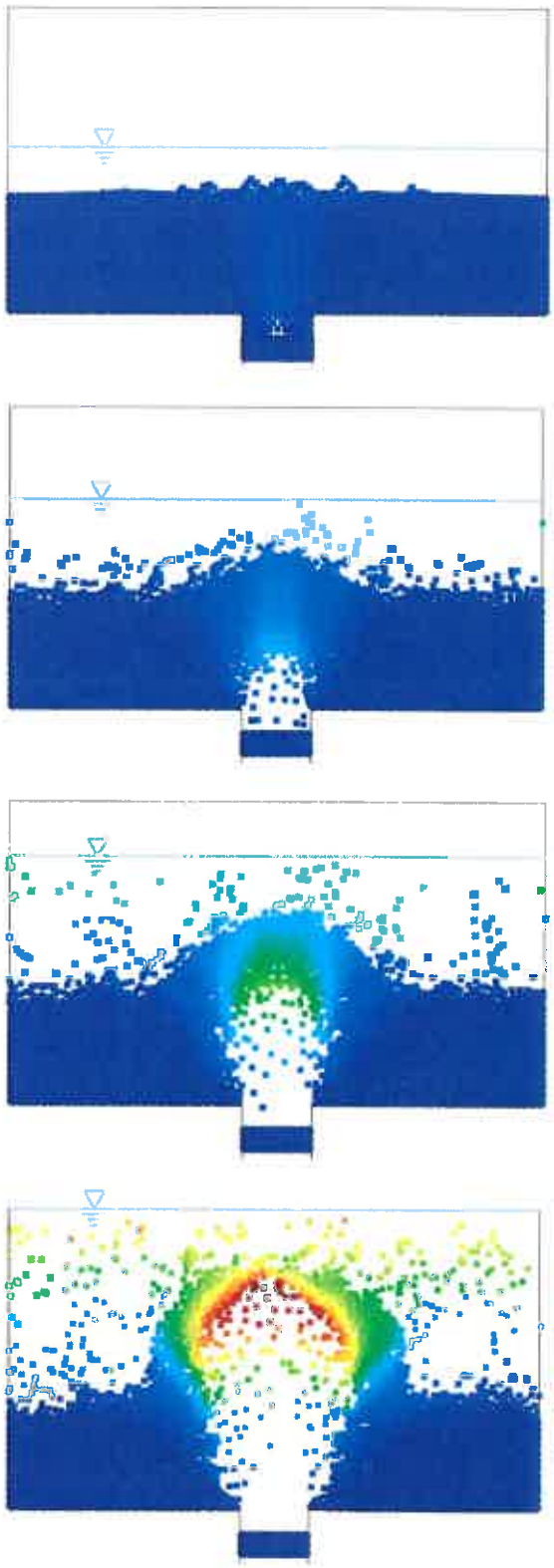

Figure 7: Displacement of soil grains at different time stages where the water particles are turned off to focus on the behaviour of sand (dark blue zero with dark red 0.216 [m])

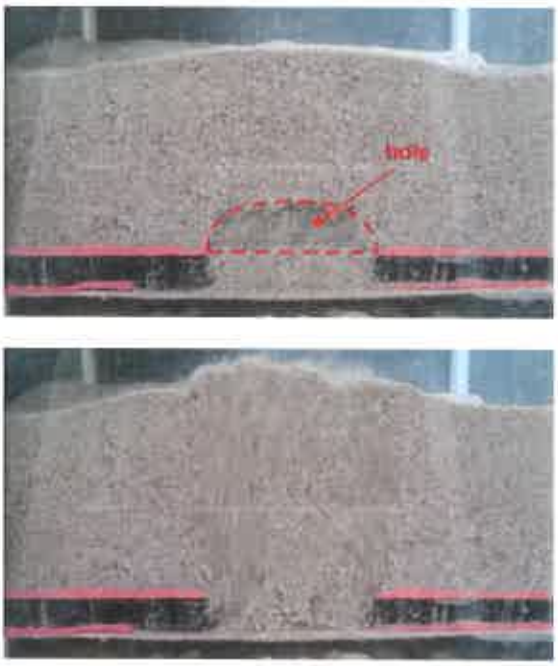

Figure 8: Experimental investigations of hydraulic heave (Brandt 2015)

References

Alsaydalani, M.O.A. & Clayton, C.R.I. (2014). *Internal fluidization in granular soils*, Journal of Geotechnical and Geoenvironmental Engineering 140, 04013024-1–04013024-10.

Aulbach, B. (2013). *Hydraulic heave: the required embedded length for construction pits in non-cohesive soil*, RWTH Aachen University, Institute of Geotechnical Engineering, Aachen, Germany.

Bandara, S. (2013). *Material point method to simulate large deformation problems in fluid-saturated granular medium*, University of Cambridge, Geotechnical and Environmental Research Group, England.

Benmebarek, N., Benmebarek, S. & Kastner, R. (2005). *Numerical studies of seepage failure of sand within a cofferdam*, Computers and Geotechnics 32, 264–273.

Bolognin, M., Martinelli, M., Bakker, K.J. & Jonkman, S.N. (2017). *Validation of material point method for solid fluidisation analysis.* Procedia Engineering: Proceedings, 1st International Conference on the Material Point Method (Eds: Rohe, A., Soga, K., Teunissen, H. & Coelho, B.Z.), 233-241. Elsevier Ltd., Amsterdam, Netherlands.

Brandt, R. (2015). *Simulation von hydraulischen Versagenszuständen bei Imperfektionen in wasserdichten Baugrubenkonstruktionen*, University of Stuttgart, Institute of Geotechnical Engineering, Master Thesis, Stuttgart, Germany.

Cheng, A.H.D. & Detournay, E. (1988). *A direct boundary element method for plane strain poroelasticity*, International Journal for Numerical and Analytical Methods in Geomechanics 12, 551–572.

Fonte, J.B. (2010). *Numerical modeling of excavations below the water table*, Universidade do Porto, Geotechnics Division, Master Thesis, Porto, Portugal.

Grabe, J. & Stefanova, B. (2015). *Numerical modeling of saturated soils based on smoothed particle hydrodynamics (SPH) Part 2: Coupled analysis*, Geotechnik 38, 218–229.

Hamad, F. (2014). *Formulation of a dynamic material point method and applications to soil-water-geotextile systems*, University of Stuttgart, Institute of Geotechnical Engineering, Germany.

Jassim, I. (2013). *Formulation of a dynamic material point method for geomechanical problems*, University of Stuttgart, Institute of Geotechnical Engineering, Germany.

Koltuk, S. (2017). *Investigations on the seepage failure by heave in excavation pits in non-cohesive soils*, RWTH Aachen University, Institute of Geotechnical Engineering, Germany.

Schober, P. (2015). *Zum hydraulischen Grundbruch an Baugrubenumschließungen bei luftseitiger Sicherung durch einen Auflastfilter in nichtbindigen Böden*, Bundeswehr University Munich, Institute of Soil Mechanics and Foundation Engineering, Munich, Germany.

Sulsky, D. & Schreyer, H.L. (1996). *Axisymmetric form of the material point method with applications to upsetting and tylor impact problems*, Journal Computer Methods in Applied Mechanics and Engineering 139, 409–429.

Sulsky, D. Zhou, S.J. & Schreyer, H.L. (1995). *Application of a particle-in-cell method to solid mechanics*, Computer Physics Communications 87, 236–252.

Terzaghi, K. (1925). *Erdbaumechanik*, Deuticke, Wien, Austria.